Electronic supplementary information (ESI) for the manuscript:

The synergistic role of support surface and Au-Cu alloy in plasmonic AuCu/LDHs photocatalyst for oxidative esterification of benzyl alcohol with methanol

Xiaoyu Wang,[a,b] Ruiyi Wang,*[a] Jie Wang,[a,b] Chaoyang Fan[a,c] and Zhanfeng Zheng*[a,b]

[a] *State Key Laboratory of Coal Conversion, Institute of Coal Chemistry, Chinese Academy of Sciences, Taiyuan, Shanxi 030001, PR China*

[b] *Center of Materials Science and Optoelectronics Engineering, University of Chinese Academy of Sciences, Beijing 100049, PR China*

[c] *Taiyuan University of Technology, Taiyuan, 030024, PR China*

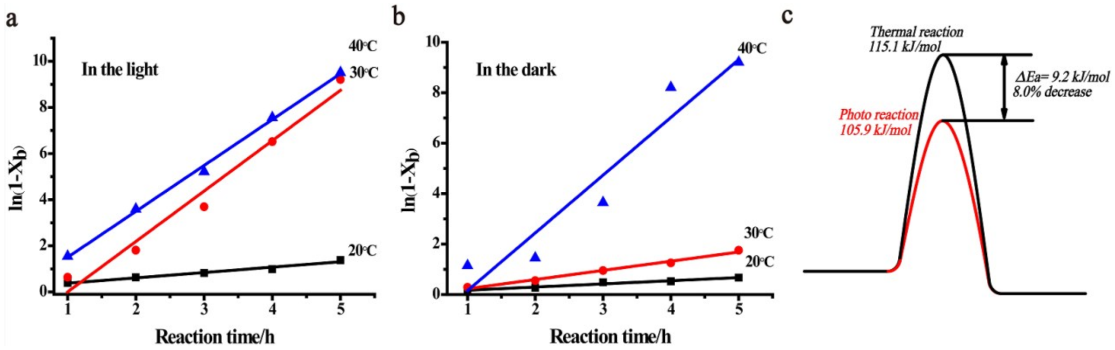

Figure S1. (a) Plot of ln (1−X_b) versus reaction time at different temperatures on the $Au_2Cu@Mg_3Al$-LDHs photocatalyst: the reaction was conducted in light or (b) in the dark, and (c) the activation energy scheme.

As an important feature of the photocatalytic process on the $Au_2Cu@MgAl$-LDHs photocatalysts, the kinetics data of photocatalytic reaction under various temperatures and the apparent activation energy by using the Arrhenius equation were conducted. As shown in Fig. S1a, b, the values of the slopes calculated from the kinetic plots are equal to the negative value of the rate constant k. According to the Arrhenius equation, two straight lines of ln k versus (1/T) were obtained, from which the activation energies of photocatalytic reaction and in the dark could be derived as the value of the slope is -Ea/R. Then the activation energies of light-driven (denoted as Eap) and thermal-driven (denoted as Ead) reaction were calculated according to the Arrhenius equation, as shown in Fig. S1c, being 105.9 and 115.1 kJ·mol^{-1} respectively. From these results, which means that 9.2 kJ·mol^{-1} (ΔEa=Ead-Eap) is reduced by visible irradiation. The result evidenced that light energy can facilitate the reaction.[1]

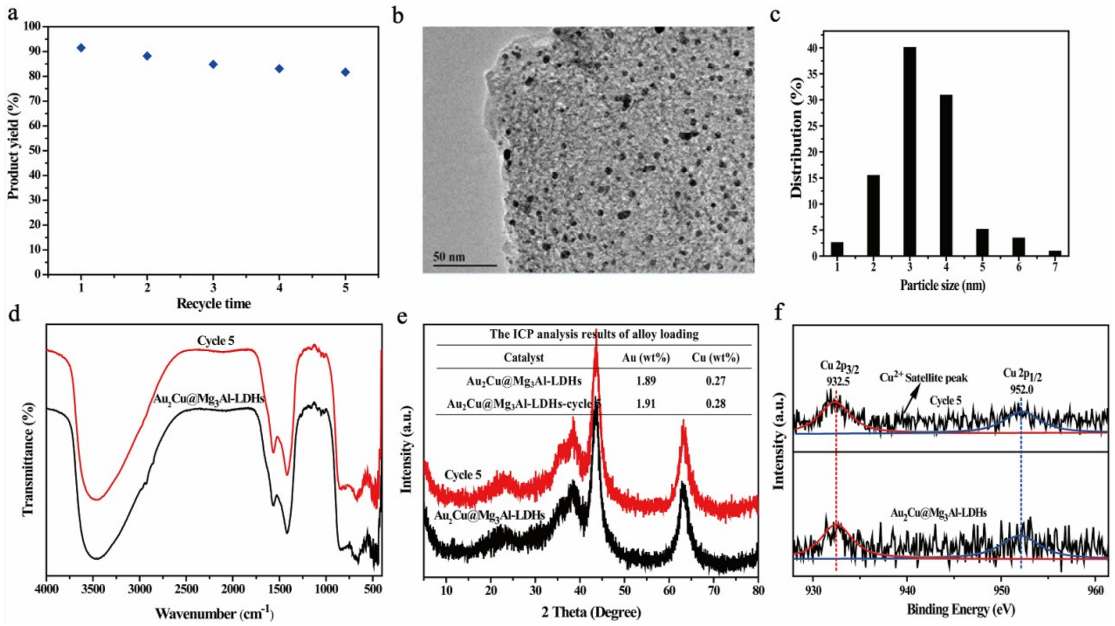

The ICP analysis results of alloy loading

Catalyst	Au (wt%)	Cu (wt%)
$Au_2Cu@Mg_3Al$-LDHs	1.89	0.27
$Au_2Cu@Mg_3Al$-LDHs-cycle 5	1.91	0.28

Figure S2. (a) Recyclability of $Au_2Cu@Mg_3Al$-LDHs photocatalyst in the oxidative esterification of benzyl alcohol for five cycles. (b) Representative TEM image of the $Au_2Cu@Mg_3Al$-LDHs photocatalyst after being recycled. (c) Particle size distribution of the NPs based on the statistical analysis of TEM images after being recycled. (d) FT-IR spectra and (e) X-ray diffraction (XRD) patterns of the purified $Au_2Cu@Mg_3Al$-LDHs and the $Au_2Cu@Mg_3Al$-LDHs used after five times. (f) XPS profiles of Cu species in $Au_2Cu@Mg_3Al$-LDHs and $Au_2Cu@Mg_3Al$-LDHs used after five times.

As shown in Fig. S2a, the $Au_2Cu@Mg_3Al$-LDHs photocatalyst was reused for five cycles with slightly decreased of product yield. From the TEM image of the $Au_2Cu@Mg_3Al$-LDHs catalyst after being recycled (Fig. S2b and 2c), there is no obvious agglomeration of the alloy NPs. The FT-IR spectra of of fresh and used catalysts under oxygen show that no changes of surface functional groups of photocatalyst in the recycle experiments (Fig. S2d). Besides, it was found that there is no obvious structure change after the reaction according to the XRD patterns of the sample after 5 cycles (Fig. S2e). The XPS profiles indicated that Cu^0 is the main state of Cu in the $Au_2Cu@Mg_3Al$-LDHs catalyst after five cycles, although there is a little of Cu^{2+} state appeared due to the characteristic Cu^{2+} shakeup satellite peaks (938-945 eV) are displayed shown in Fig. S2f, the slight decline in the photocatalytic activity of $Au_2Cu@Mg_3Al$-LDHs during the cycling experiment may be due to a small amount of Cu were oxidated during the catalytic cycle process.

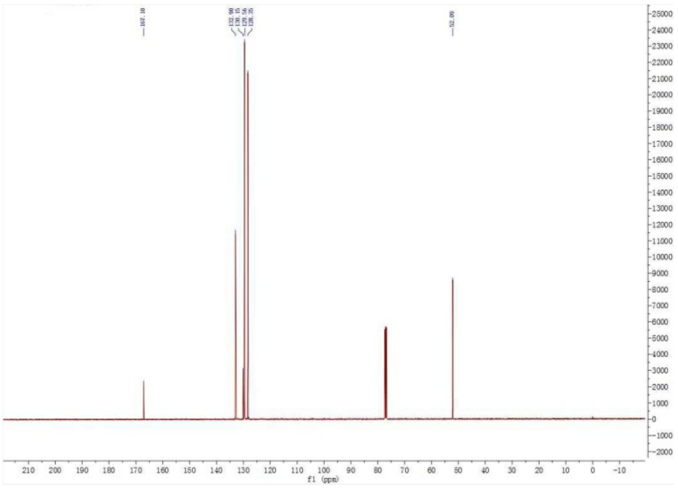

Figure S3. ^{13}C NMR (125MHz, $CDCl_3$, TMS) spectrum of methyl benzoate: δ 52.09, 128.35, 129.56, 130.15, 132.90, 167.10.

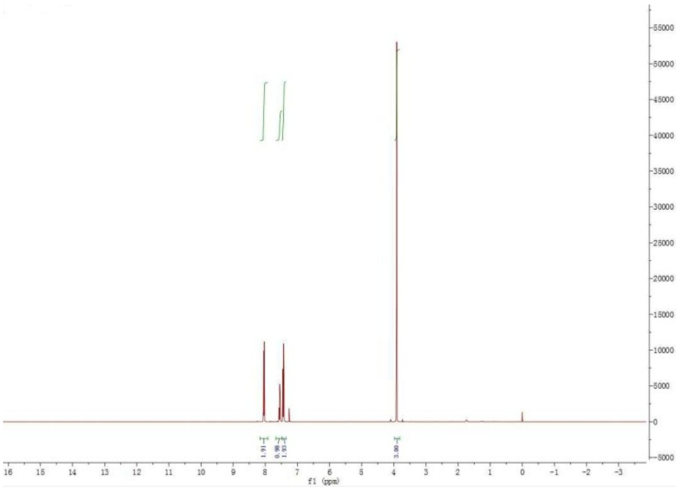

Figure S4. ^{1}H NMR (500MHz, $CDCl_3$, TMS) spectrum of methyl benzoate: δ 3.91 (s, 3H), 7.45 (t, 2H), 7.57 (t, 1H), 8.05 (d, 2H).

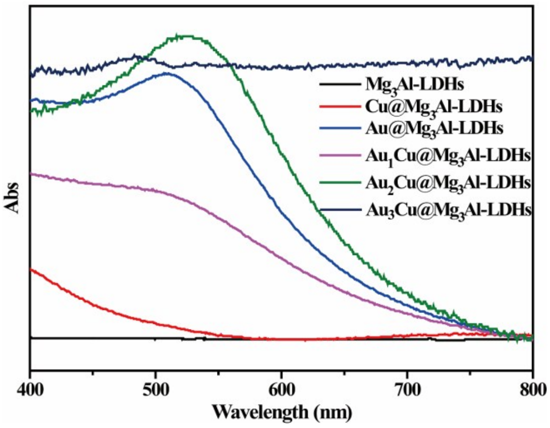

Figure S5. UV-Vis spectra of the Au-Cu alloy catalysts.

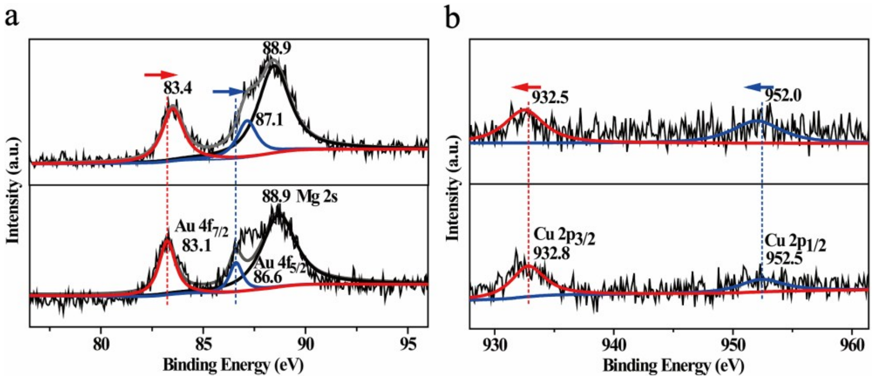

Figure S6. (a) Au 4f XPS spectra of $Au_2Cu@Mg_3Al$-LDHs (up) and $Au@Mg_3Al$-LDHs (down). (b) Cu 2p XPS spectra of $Au_2Cu@Mg_3Al$-LDHs (up) and $Cu@Mg_3Al$-LDHs (down).

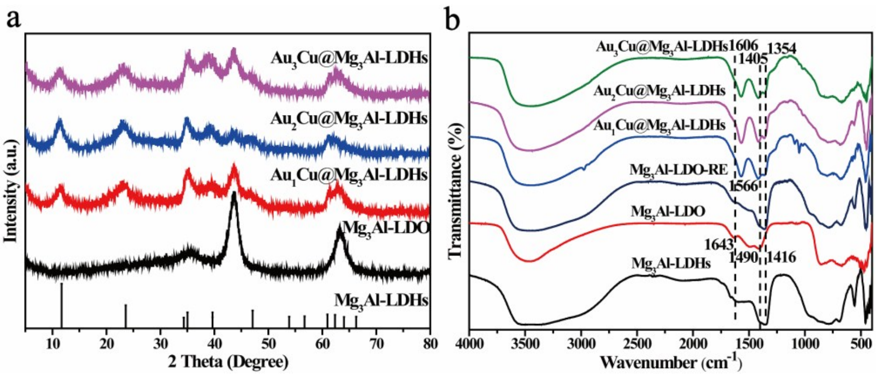

Figure S7. (a) XRD patterns of the samples. (b) FT-IR spectra of samples (Mg_3Al-LDO-RE: reconstruction of Mg_3Al-LDHs).

To characterize the crystalline phase of Au-Cu@Mg_3Al-LDHs samples, the XRD patterns are shown in Fig. S7a. After loading Au-Cu alloy NPs, the Au-Cu@Mg_3Al-LDHs samples exhibit both hydrotalcite-like structure and the corresponding oxides structure (JCPDS No. 45-0946) ascribed to the memory effect of hydrotalcite. Besides, no reflections appeared ascribed to the Au-Cu NPs in the XRD patterns, which may due to the low metal content was below the detection limit and the uniform distribution of the metal NPs on the surface of LDHs. Moreover, the FT-IR spectra of Au-Cu@Mg_3Al-LDHs samples are collected shown in Fig. S7b. The broad band centred around 3500 cm^{-1} is assigned to a complex of overlapping stretching modes of the hydroxyl groups present in the brucite-type layer and the interlayer water molecules. The band at 1643 cm^{-1} is associated with the deformation mode of the hydroxyl groups. The bands at 1354 cm^{-1} and 1405 cm^{-1} are assigned to the carbonate species antisymmetric stretching modes. Several bands below 1000 cm^{-1} are associated with the M-O vibrational modes (Mg-O, Al-O) in the brucite-type layer.[2] After calcinated at 450 °C (Mg_3Al-LDO), all the bands of hydroxyl groups and carbonate species decrease in intensity and high frequency shift ascribed to the desorption of H_2O and CO_2 of Mg_3Al-LDHs with in the thermal treatment. After loading Au-Cu alloy NPs, the bands of hydroxyl groups and carbonate species increase in intensity and low frequency shift ascribed to the memory effect of hydrotalcite (reconstruction of hydrotalcite), which shows good agreement with the XRD results. In addition, after loading Au-Cu alloy NPs samples showing a more intense the shoulder band at 1566 cm^{-1}, which is assigned to the splitting asymmetric stretching band of interlayer carbonate due to lowering of local symmetry of carbonate in the interlayer, as compared to Mg_3Al-LDHs and Mg_3Al-LDO. It may be due to a small amount of Au-Cu alloy ions interacted with carbonate ions lowering the local symmetry of carbonate.[3] Generally, there are little effect on the structural and textural properties of Mg_3Al-LDHs after loading Au-Cu alloy NPs.

Table S1 Physical characteristics of samples.

catalyst	$S_{BET}(m^2 \cdot g^{-1})$[a]	$V_P(cm^3 \cdot g^{-1})$[b]	$D_P(nm)$[c]
$Au_2Cu@Mg_3Al$-LDHs	206.5954	0.753564	9.0669
$Au_1Cu@Mg_3Al$-LDHs	297.5157	0.855804	8.0731
$Au_3Cu@Mg_3Al$-LDHs	298.5018	0.822711	8.0583
$Au@Mg_3Al$-LDHs	180.0040	0.808717	8.3690
$Cu@Mg_3Al$-LDHs	218.1853	0.662808	7.9237
Mg_3Al-LDO-RE	73.3806	0.392527	15.6951
Mg_3Al-LDHs	23.8221	0.069155	15.3135
Mg_3Al-LDO	206.2228	0.198357	5.1865
$Au_2Cu@MgO$	85.8098	0.490819	18.6966
$Au_2Cu@\ Al_2O_3$	137.8159	0.246232	5.4165
$Au_2Cu@Mg_3Al$-LDHs[d]	26.5629	0.085095	15.0932
$Au_2Cu@Mg_2Al$-LDHs	176.2453	0.734964	8.4781
$Au_2Cu@Mg_1Al$-LDHs	280.0040	0.783811	9.6382
$Au_2Cu@Zn_2Al$-LDHs	53.8068	0.269259	20.3676

a. Specific surface area; b. Total pore volume; c. Average pore diameter; d. Direct loading of Au-Cu alloy NPs onto HT.

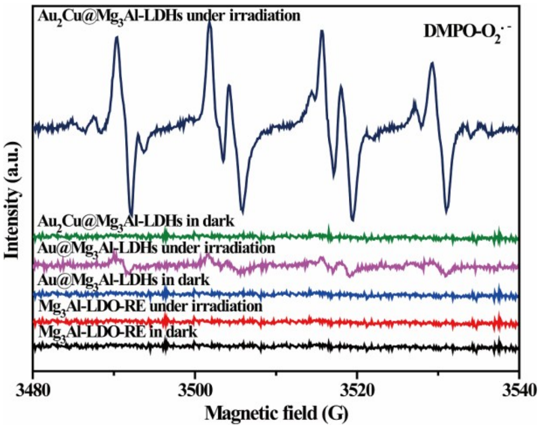

Figure S8. ESR spectra of radical adducts trapped by DMPO (DMPO-$O_2^{\cdot-}$) in the Au_2Cu@Mg_3Al-LDHs, Au@Mg_3Al-LDHs and Mg_3Al-LDO-RE dispersion solution (solvent was DMSO) under irradiation and in the dark.

Table S2. Photocatalytic Oxidative Esterification of Benzyl Alcohol with Methanol over Au-Cu alloy NPs with Varied Supports [a]

entry	**catalyst**	**incident light**	**conversion (%)**	**selectivity (%)**	**yield (%)**	**TOF (s^{-1})**
1	Au_2Cu@Mg_3Al-LDHs	visible	97.0	99.4	96.4	0.048
		dark	61.3	97.0	59.5	0.029
2	Au_2Cu@MgO	visible	51.6	96.0	49.5	0.030
		dark	30.2	91.8	27.7	0.018
3	Au_2Cu@Al_2O_3	visible	31.8	76.1	24.2	0.014
		dark	14.3	67.7	9.7	0.0063
4	Au_2Cu@MgO+Au_2Cu@Al_2O_3 [c]	visible	32.2	78.2	25.2	---
		dark	14.5	77.0	11.2	---
5	Au_2Cu@Mg_3Al-LDHs [d]	visible	24.0	84.3	20.2	0.010
		dark	14.9	69.1	10.3	0.0062
6	Au_2Cu@Mg_2Al-LDHs	visible	63.8	98.2	62.7	0.033
		dark	52.1	94.1	49.0	0.027
7	Au_2Cu@Mg_1Al-LDHs	visible	53.2	97.4	51.8	0.028
		dark	33.3	67.4	22.4	0.017
8	Au_2Cu@Zn_2Al-LDHs [e]	Xe light	27.5	64.2	17.7	0.0070
		dark	41.9	85.6	35.9	0.010
9	Au_2Cu@Zn_2Al-LDHs [f]	visible	56.3	94.7	53.3	0.014
10	Au_2Cu@Zn_2Al-LDHs [g]	dark	25.2	59.3	14.9	0.0064

a. Reaction conditions: photocatalyst, 10 mg; benzyl alcohol, 0.5 mmol; methanol, 5 ml; K_2CO_3, 0.2 mmol; O_2, atmospheric pressure; reaction temperature, 30 °C; reaction time, 3 h; light intensity (cut420 of Xe lamp), 0.5 $W\cdot cm^{-2}$; b. Specific surface area; c. Au_2Cu@MgO and Au_2Cu@Al_2O_3 were mechanically mixed in a motar according to n(Mg): n(Al)=3:1; d. Direct loading of Au-Cu alloy NPs onto HT; e. Reaction time, 6 h and light source, full-spectrum Xe lamp (0.5 $W\cdot cm^{-2}$); f. reaction time, 6 h; g. the reaction was conducted in the dark using the catalyst which has been irradiated under full-spectrum Xe lamp for 6 h.

Table S3 The ICP analysis results of Mg/Al ratios in LDHs

Catalyst	Mg (mg/L)	Al (mg/L)	Mg/Al (molar ratio)
$Au_2Cu@Mg_1Al$-LDHs	14.20	17.18	0.93
$Au_2Cu@Mg_2Al$-LDHs	20.29	12.44	1.83
$Au_2Cu@Mg_3Al$-LDHs	23.56	9.93	2.67

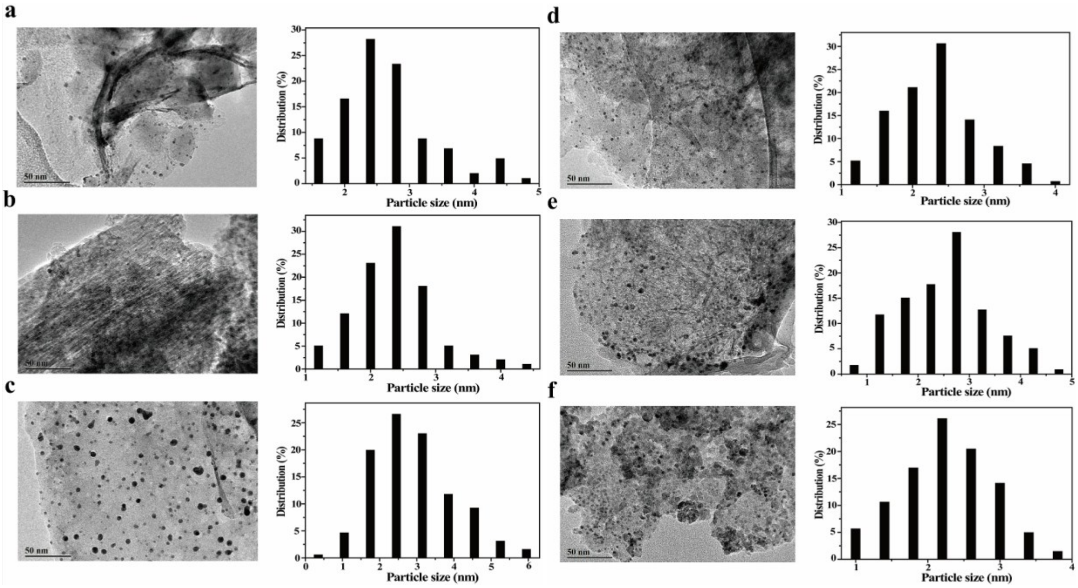

Figure S9. TEM images of the Au-Cu alloy NPs with varied supports samples and particle size distribution of the NPs based on the statistical analysis of TEM images: (a) Au_2Cu@MgO (b) Au_2Cu@Al_2O_3 (c) Au_2Cu@Mg_3Al-LDHs (direct loading of Au-Cu alloy NPs onto HT) (d) Au_2Cu@Mg_2Al-LDHs (e) Au_2Cu@Mg_1Al-LDHs (f) Au_2Cu@Zn_2Al-LDHs.

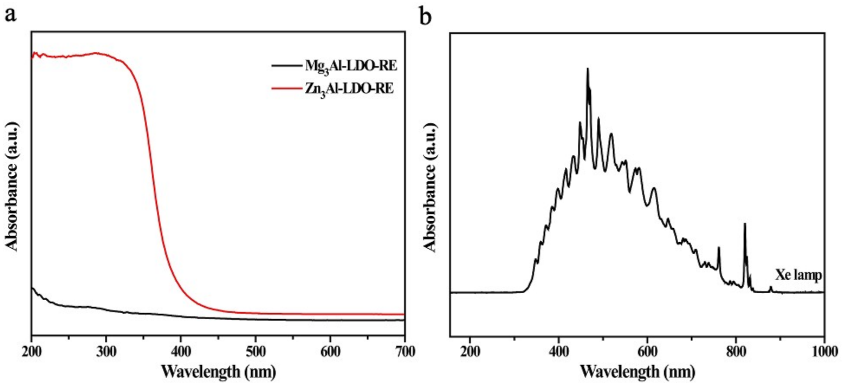

Figure S10. (a) UV-Vis spectra of Mg_3Al-LDO-RE and Zn_3Al-LDO-RE. (b) Output spectra of full-spectrum Xe lamp.

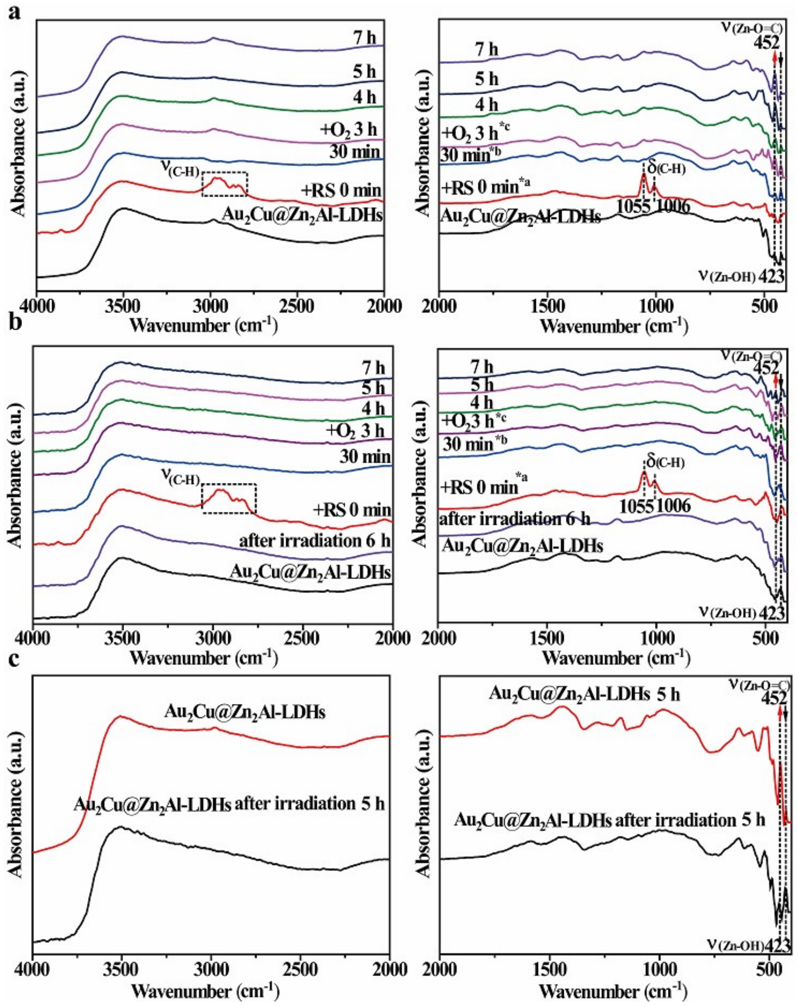

Figure S11. *In-situ* FT-IR spectra of (a) Au$_2$Cu@Zn$_2$Al-LDHs after co-adsorption of benzyl alcohol and methanol (*a: dropping the reaction solution of 0.5 mmol benzyl alcohol, methanol as solvent; *b: after argon purge for 30 min; *c: pass in oxygen and start to heat up for 3 h). (b) Au$_2$Cu@Zn$_2$Al-LDHs which was irradiated under full-spectrum Xe lamp for 6 h, then co-adsorption of benzyl alcohol and methanol. (c) Comparison between no irradiated photocatalyst and after irradiated under full-spectrum Xe lamp for 6 h photocatalyst which after co-adsorption of benzyl alcohol and methanol for 5 h.

As shown in Fig. S11a,b, whatever the no irradiated photocatalyst or after irradiated under full-spectrum Xe lamp for 6 h photocatalyst, the vibrational modes band of Zn-OH at 423 cm^{-1} [4] are both decresed in intensity indicating that dehydroxylation of Zn-OH of support Zn$_2$Al-LDHs during the reaction. Meanwhile, a new vibrational modes band of Zn-O at 452 cm^{-1} are both appeared, incresed in intensity during the reaction and blue frequency shift compared to the IR spectra of Zn-OH in support Zn$_2$Al-LDHs, which also indicate the formation of Zn-O=C after the dehydroxylation of Zn-OH due to the adsorption of alcohol molecules on the basic sites of support by the oxygen, then the intermediate aldehyde is formed because of the dehydrogenated of alcohol during the reaction. Besides, as shown in Fig. S11c, the new band intensity of Zn-O=C (452 cm^{-1}) is apparently stronger in no irradiated photocatalyst system compared to the photocatalyst system after irradiated under full-spectrum Xe lamp. It is conclued that the increase of the surface hydroxyl group after irradiation inhibited the adsorption of alcohol molecules due to that the increase of the hydroxyl group means the distance between hydroxyl groups becomes smaller, which inhibits the adsorption of alcohol molecules because of the steric hindrance effect, which ultimately results in a decrease in activity.

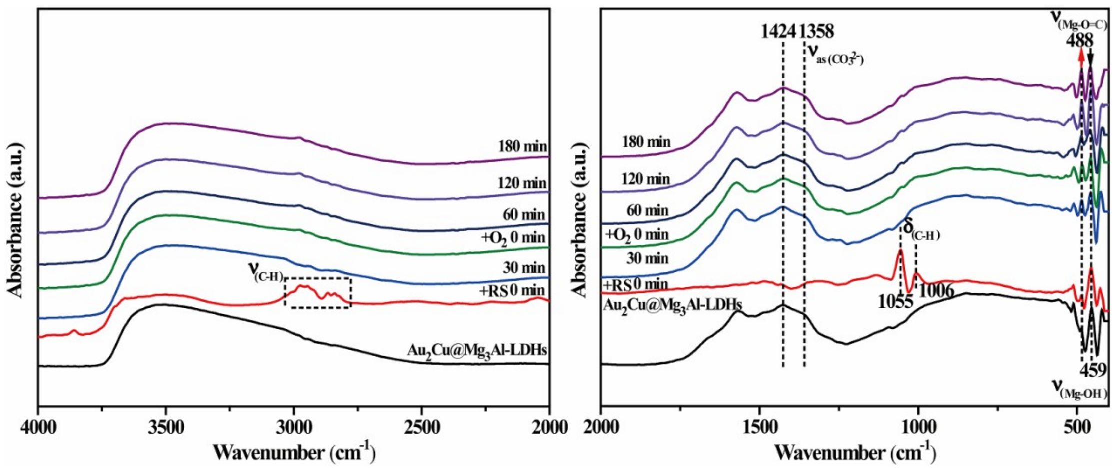

Figure S12. *In-situ* FT-IR spectra of $Au_2Cu@Mg_3Al$-LDHs after co-adsorption of benzyl alcohol and methanol.

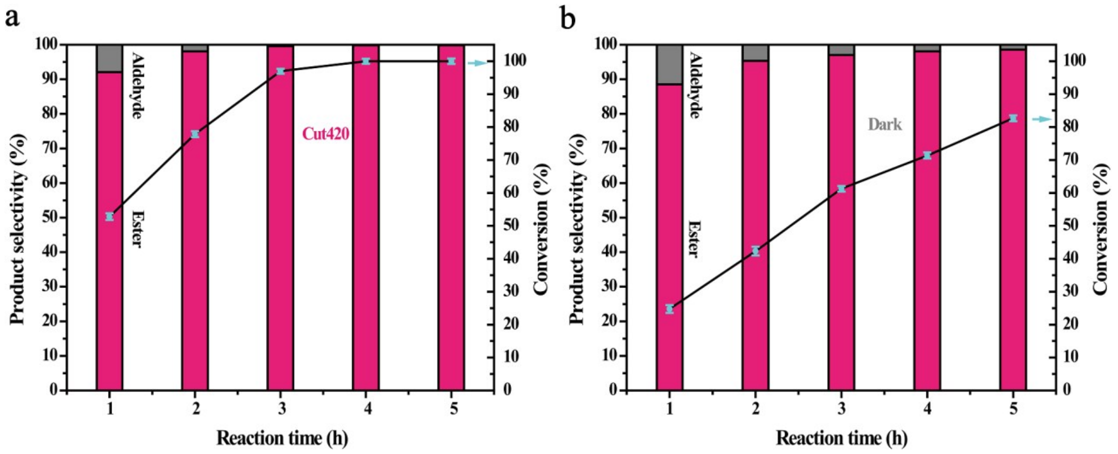

Figure S13. (a) The catalytic activities of the oxidative esterification of benzyl alcohol using $Au_2Cu@Mg_3Al$-LDHs photocatalyst at different times under visible-light irradiation and (b) in the dark. Reaction conditions: photocatalyst, 10 mg; benzyl alcohol, 0.5 mmol; methanol, 5 ml; K_2CO_3, 0.2 mmol; O_2, atmospheric pressure; reaction temperature, 30 °C; light intensity (cut420 of Xe lamp), 0.5 W·cm^{-2}.

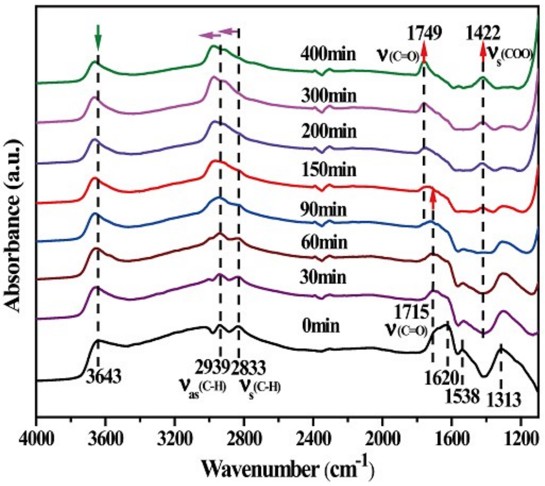

Figure S14. *In-situ* FT-IR spectra of $Au_2Cu@Mg_3Al$-LDHs after co-adsorption of benzyl alcohol and methanol (deduction of IR spectra of $Au_2Cu@Mg_3Al$-LDHs).

In-situ FT-IR spectra after coadsorption of benzyl alcohol and methanol on $Au_2Cu@Mg_3Al$-LDHs shown in Fig. S14. Band at 3643 cm^{-1} is typical band of the O-H stretching vibrations of benzyl alcohol and methanol, which proportionally diminished in intensity indicating that hydroxyl of benzyl alcohol and methanol has been dehydrogenated by the cleavage of the O-H bond.[5] Bands at 2939 cm^{-1} and 2833 cm^{-1} are typical bands of the C-H stretching vibrations of methylene of benzyl alcohol and methyl of methanol. The absorption band at 1620 cm^{-1}, 1538 cm^{-1} and 1313 cm^{-1} are assigned to the carbon-carbon double bond and C-H bond deformation vibrations of the aromatic ring of benzyl alcohol,[6] which gradually decreased in intensity indicate that part of the benzyl alcohol has desorbed after the reaction process.[7]

A new band at 1715 cm^{-1} was appeared and increased in intensity which assigned to the -C=O- bond stretching vibrations of benzaldehyde when the reaction time were conducted from 0 min to 90 min indicating the intermediate product benzaldehyde was firstly generated during the catalytic process.[8] Blue frequency shift of this band compared to the IR spectra of neat benzaldehyde (1710-1630 cm^{-1}) indicate the carbonyl oxygen atoms of benzaldehyde associated with the base sites of support due to the coordination of C-H of benzaldehyde with unsaturated Au-Cu alloy NPs active sites to form a metal-H bond can result in the C=O bond length of benzaldehyde decreasing, which provided another favourable evidence that benzyl alcohol molecular associated with the basic sites of support at the begaining of catalytic reaction, rather than associated with the Au-Cu alloy NPs active sites because of the red shift of the C=O bond is expected with respect to neat benzaldehyde if benzyl alcohol molecular associated with the Au-Cu alloy NPs active sites due to the coordination of carbonyl oxygen atoms with metal atoms can result in the bond length increasing. It is noteworthy that this band also appeared at 0min which might due to the reaction has been conducted, once the reactants adsorbed on the surface of catalyst. Besides, the proportionally decreased in intensity of C-H stretching vibrations band at 2939 cm^{-1} and 2833 cm^{-1} indicating that the cleavage of the C-H bond of methylene of benzyl alcohol during the catalytic process.

The bands at 1749 cm^{-1} and 1422 cm^{-1} was appeared and increased in intensity which assigned to the -C=O- bond stretching vibrations and -COO- bond stretching vibrations of methyl benzoate respectively [9] when the reaction time were conducted from 90 min to 400 min indicating that methyl benzoate was then generated after nucleophilic attack at the carbonyl carbon of intermediate product benzaldehyde by methoxy of methanol. Blue frequency shift of this band compared to the IR spectra of neat methyl benzoate (1730-1725 cm^{-1}) indicate the carbonyl oxygen atoms of methyl benzoate associated with the base sites of support of photocatalyst. Meanwhile, the blue frequency shift of C-H stretching vibrations band at 2939 cm^{-1} and 2833 cm^{-1} indicating that the inductive effect of C-OCH_3 band was generated due to the nucleophilic addition of methoxy of methanol with carbonyl carbon can result in the bond length decreasing.

Table S4 The carbon balance of reaction.

Catalyst		Conv. (%)	Carbon balance (%)
$Au_2Cu@Mg_3Al$-LDHs	light	97.0	99.0
	Dark	61.3	97.9
$Au_1Cu@Mg_3Al$-LDHs	light	17.4	96.6
	Dark	14.5	99.3
$Au_3Cu@Mg_3Al$-LDHs	light	74.8	98.9
	Dark	42.7	98.4

Reaction conditions: photocatalyst, 10 mg; benzyl alcohol, 0.5 mmol; methanol, 5 ml; K_2CO_3, 0.2 mmol; O_2, atmospheric pressure; reaction temperature, 30 °C; reaction time, 3 h; light intensity (cut420 of Xe lamp), 0.5 $W\cdot cm^{-2}$.

Calculation details of carbon balance (CB): $CB = [N_{\text{methyl benzoate}} \times n_{\text{methyl benzoate}}/(N_{\text{benzyl alcohol}} \times n_{\text{benzyl alcohol}} + N_{\text{methanol}} \times n_{\text{methanol}}) \times X\%] \times 100\%$, where $N_{\text{benzyl alcohol}}$, N_{methanol} and $N_{\text{methyl benzoate}}$ are the carbon number of benzyl alcohol, methanol and methyl benzoate respectively, $n_{\text{benzyl alcohol}}$, n_{methanol} and $n_{\text{methyl benzoate}}$ are the mole number of benzyl alcohol, methanol and product formed respectively, X% is the conversion of benzyl alcohol (n_{methanol} is equal to $n_{\text{benzyl alcohol}}$ due to the amount of methanol added is excessive).

Notes and references

(1) S. Sarina, E. R. Waclawik and H. Zhu, *Green Chem.*, 2013, **15**, 1814-1833.

(2) L. Hickey, J. T. Kloprogge, R. L. Frost, *J. Mater. Sci.*, 2000, **35**, 4347-4355.

(3) M. Dixit, M. Mishra, P. A. Joshi, D. O. Shah, *J. Ind. Eng. Chem.*, 2013, **19**, 458-468.

(4) R. V. Jagadeesh, H. Junge, M. M. Pohl, J. Radnik, A. Brückner and M. Beller, *J. Am. Chem. Soc.*, 2013, **135**, 10776-10782.

(5) T. Ebata, T. Watanabe and N. Mikami, *J. Phys. Chem.*, 1995, **99**, 5761-5764.

(6) E. B. WiLsoN, *Phys. Rev.*, 1934, **45**, 706-714.

(7) T. Beutel, *J. Chem. Soc., Faraday Trans.*, 1998, **94**, 985-993.

(8) D. M. Meier, A. Urakawa and A. Baiker, *J. Phys. Chem. C.*, 2009, **113**, 21849-21855.

(9) N. Sundaraganesan, B. D. Joshua, *Spectrochim. Acta, Part A*, 2007, **68**, 771-777.